Water Resources Research

RESEARCH ARTICLE
10.1029/2019WR026619

Defining a Riverine Tidal Freshwater Zone and Its Spatiotemporal Dynamics

Allan E. Jones[1,2], Amber K. Hardison[3], Ben R. Hodges[4], James W. McClelland[3], and Kevan B. Moffett[2]

[1]Department of Geological Sciences, University of Texas at Austin, Austin, TX, USA, [2]School of the Environment, Washington State University Vancouver, Vancouver, WA, USA, [3]Marine Science Institute, University of Texas at Austin, Port Aransas, TX, USA, [4]Department of Civil, Architectural and Environmental Engineering, University of Texas at Austin, Austin, TX, USA

Key Points:
- Established measurable definition of tidal freshwater zone (TFZ) and observed and analyzed tidal freshwater zone in Texas, USA
- Median zone length was 59.9 km in Aransas River, TX, USA, with late summer maximum length of 66.0 km and a winter minimum of 53.6 km
- Runoff events lengthened and seasonal drought shortened the zone, which was also mobile along channel due to changing tide and climate

Supporting Information:
- Supporting Information S1

Correspondence to:
A. E. Jones,
allan.e.jones@utexas.edu

Citation:
Jones, A. E., Hardison, A. K., Hodges, B. R., McClelland, J. W., & Moffett, K. B. (2020). Defining a riverine tidal freshwater zone and its spatiotemporal dynamics. *Water Resources Research*, *56*, e2019WR026619. https://doi.org/10.1029/2019WR026619

Received 24 OCT 2019
Accepted 15 MAR 2020
Accepted article online 17 MAR 2020

Abstract Tidal freshwater zones (TFZs) are transitional environments between terrestrial and coastal waters. TFZs have freshwater chemistry and tidal physics, and yet are neither river nor estuary based on classic definitions. Such zones have been occasionally discussed in the literature but lack a consistent nomenclature and framework for study. This work proposes a measurable definition for TFZs based on three longitudinal points of interest: (1) the upstream limit of brackish water, (2) the upstream limit of bidirectional tidal velocities, and (3) the upstream limit of tidal stage fluctuations. The resulting size and position of a TFZ is transient and depends on the balance of tidal and riverine forces that evolves over event, tidal, seasonal, and annual (or longer) timescales. The concept, definition, and transient analysis of TFZ position are illustrated using field observations from the Aransas River (Texas, USA) from July 2015 to July 2016. The median Aransas TFZ length was 59.9 km, with a late summer maximum of 66.0 km and a winter minimum of 53.6 km. The TFZ typically (annual median) began 11.8 km upstream from the river mouth (15.4 km winter/11.2 km summer medians) and ended 71.7 km upstream (69.0 km/77.2 km). Seasonally low baseflow in the Aransas River promoted gradual coastal salt encroachment upstream, which shortened the TFZ. However, sporadic large rainfall/runoff events rapidly elongated the TFZ. The TFZ definition establishes a quantifiable framework for analyzing these critical freshwater systems that reside at the nexus of natural and human-influenced hydrology, tides, and climate.

Plain Language Summary Rivers reaching the coast begin to feel the impact of tides. Coastal river segments can rise and fall with the tide and even flow inland at certain times during the tidal cycle. At the same time, the tide can push salty coastal water upstream, traveling from offshore up the river channel. This study focuses on the river segment between that salty water and freshwater flowing toward the coast. This region of the river is the "tidal freshwater zone," (TFZ) because this river water is both fresh, meaning it contains effectively no salt, and tidal, since it moves with the tide. In this paper, we define the key characteristics of a TFZ, and observe one of these zones in a coastal river in Texas over 1 year. We witnessed the TFZ expand and shrink like an accordion as rain events added more freshwater, and droughts removed freshwater allowing the tide to push salt water upstream quickly. We also observed the zone move back and forth along the river channel as the seasons and climate changed. Future coastal water management plans should account for the TFZ since this river segment may move vital nutrients to the coast very slowly. Also, climate change may strongly impact TFZs, since these zones are influenced by two major consequences of climate change: rising sea level (i.e., tide) and rising temperatures (i.e., altered water cycle).

1. Introduction

Riverine freshwater discharge is critically important in estuarine and coastal ecology. In low relief coastal river reaches, transitional environments along a river-estuary continuum experience the interaction of hydrology and tides well upstream of the brackish estuarine waters. These freshwater transitional environments are thought to play a role in controlling the timing and magnitude of nutrient and freshwater fluxes to coastal ecosystems, and hence coastal productivity (Arndt et al., 2007, 2011; Brock, 2001; Bruesewitz et al., 2013; Dyer, 1997; Ensign et al., 2008; Ensign, Doyle, et al., 2013; Knights et al., 2017; Mooney &

McClelland, 2012; Palmer et al., 2002, 2011; Pollack et al., 2011; Savenije, 2005). Water residence times in these environments can be on the order of several months (Johnson, 2009), and these zones may exert critical controls on nutrient cycling over a coastal plain (Ensign, Siporin, et al., 2013; Knights et al., 2017; Von Korff et al., 2014). Such tidal freshwater zones (TFZs) are altered by the combined stressors of increasing coastal populations, sea level rise, and upstream hydrological controls (e.g., dams), all of which affect the balance of tide and hydrology (Destouni et al., 2008; Johnson, 2009; Neumann et al., 2015; Odum, 1988).

This work focuses on TFZs that exist along a river reach, fully upstream of the river mouth. Such TFZs exist in numerous systems worldwide. Many rivers exhibit tidal water level oscillations 10–100+ km inland, for example, the Hudson, Potomac, Scheldt, and Incomati Rivers (Arndt et al., 2011, 2007; Cole et al., 1992; Findlay et al., 1991; Lovley & Phillips, 1986a, 1986b; Savenije, 2005). Lovley and Phillips (1986a, 1986b) described a "tidal river zone" in the Potomac River (Washington, D.C., USA) that flowed into a "transition zone" and then into an "estuarine zone" and noted the consequences for the tidal river's benthic geochemistry. Ganju et al. (2004) described a "transitional regime" bordered upstream by a "river regime" and truncated downstream by a "bay regime" in the Petaluma River and Sonoma Creek (California, USA). Yankovsky et al. (2012) and Torres (2017) investigated the "freshwater transition zone" of the Santee River (South Carolina, USA). Hoitink and Jay (2016) distinguished a "tidal river" as occurring upstream of "where the lowest water levels occur on the neap rather than spring tides," and a "TFZ" as a different entity, specifically, "the entire reach between salinity intrusion and the upstream tidal boundary."

Building on the work of Cowardin et al. (1979), Odum et al. (1984) were among the first to conceptualize a "tidal freshwater" zone along the river-estuary continuum. Schuchardt et al. (1993) further discussed this intermediate riparian reach between "upstream (riverine) and downstream (mixohaline) habitats," identifying a "tidal freshwater reach." However, Ensign et al. 2008 provided an early isolation and investigation of a specific riparian segment of the river-estuary continuum as a "TFZ". Furthermore, recent studies (e.g., Ensign, Doyle, et al., 2013; Knights et al., 2017) focused on the important nutrient dynamics of an increasingly coherent and consistent "TFZ". However, a broadly accepted nomenclature and conceptual model for describing and characterizing the critical features of a TFZ has yet to be presented. Without a shared nomenclature and characterization, the community at large may not be discussing and/or analyzing the exact same environment. Longitudinal differences in physical character throughout a TFZ are vital to describing, analyzing, and understanding a TFZ's spatial impact on other environmental factors, such as biogeochemical cycling.

Several key challenges impede our understanding of the hydrological and biogeochemical nature, importance, and sensitivities of TFZs. These include the lack of (i) a consistent nomenclature to discuss such a zone and its subfeatures, (ii) a clear identification approach, and (iii) a simple, quantitative method to measure characteristics and longitudinal extent. Herein, we propose nomenclature and a classification scheme to define, describe, and empirically identify TFZs. Our approach expands on the work of Odum et al. (1984), Ensign et al. (2008), and the TFZ definition of Hoitink and Jay et al. (2016) as "the entire reach between salinity intrusion and the upstream tidal boundary." The model provided herein aims to facilitate quantitative comparisons both among coastal systems and within a single system's temporal evolution. The proposed theory and nomenclature is presented in section 2. A method for identifying TFZs and their transitional features is presented in section 3, with an aim to make the approach broadly accessible to hydrologists, aquatic ecologists, biogeochemists, and water managers. A demonstration case for applying the TFZ conceptual framework and nomenclature using field data is presented in section 4. The case study presents the year-long monitoring of a TFZ in the Aransas River of southern Texas, USA.

2. The TFZ

A TFZ is defined as *characterized by freshwater chemistry and impacted by tidal physics (i.e., bidirectional velocity and/or surface water oscillations), which is bounded downstream by a brackish water column and bounded upstream by unidirectional discharge, nontidal stage (i.e., no tidal surface water oscillations), and a fresh water column*. For our study, the TFZ must also be upstream of the river mouth. Beyond the river mouth (e.g., coastal estuary, bay, or ocean), geometry changes lead to multidimensional hydrodynamics that are more complex than channel flows (Dyer, 1997; Hoitink & Jay, 2016; Savenije, 2005; Valle-Levinson, 2010). Tidal

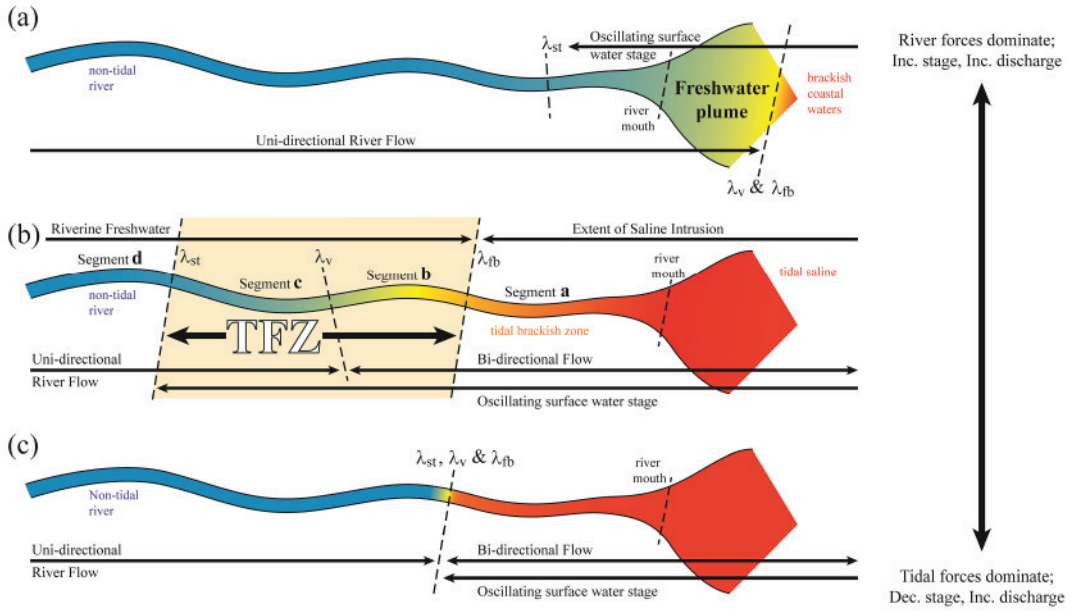

Figure 1. Theoretical spectrum of tidal freshwater zones (TFZs), as present in Figure 1b, with key transitional locations λ_{fb} (divide between fresh and brackish water column), λ_v (upstream limit of temporally alternating bidirectional discharge), and λ_{st} (upstream limit of tidal surface water stage fluctuations). In contrast, (a) a high-discharge estuary may have λ_{fb} and λ_v well downstream of the river mouth, creating a coastal freshwater plume, while (c) an estuary with strong tidal forces may position λ_{fb}, λ_v, and λ_{st} atop one another and have virtually no TFZ.

freshwaters that extend offshore (i.e., beyond the river mouth) can be called a freshwater "plume" (Figure 1a) (e.g., Beardsley et al., 1985; Fong & Geyer, 2002).

Using a conceptual, one-dimensional model of a river, we divide the riverine TFZ into four key segments based on varying degrees of tidal and riverine dominance (Figure 1b and Table 1). The critical transitions between these segments we denote as

- $\lambda_{fresh/brackish}$, or λ_{fb} – divide between *fresh* and *brackish* water column, between segments **a** and **b** in Figure 1b and Table 1;
- $\lambda_{velocity}$, or λ_v – upstream limit of *bidirectional* discharge (i.e., temporal changes in flow velocity direction from downstream to upstream and vice versa), between segments **b** and **c**; and
- λ_{stage}, or λ_{st} – upstream limit of *tidal surface water stage* fluctuations, between segments **c** and **d**

By definition, the TFZ is located between λ_{st} and λ_{fb}. Note that λ_{fb}, λ_v, and λ_{st} are not necessarily stationary in either space or time. A TFZ can exist between two extreme conditions—river dominance and estuarine dominance. At the river-dominated extreme (Figure 1a), the λ_{fb} demarcation between fresh and brackish waters may be pushed offshore of the river mouth, resulting in a freshwater plume. At the estuarine-dominated extreme, λ_{fb}, λ_v, and λ_{st} collapse to a single upstream location (Figure 1c) and the system transitions directly from riverine to estuarine without a TFZ. Between these extremes, a TFZ exists if λ_{fb}, λ_v, and λ_{st} are spread longitudinally throughout the river-estuary continuum (Figure 1b). Note that the estuarine-dominated extreme (Figure 1c) may exist primarily as a theoretical end-member, and most real-world systems likely exhibit some balance between river and estuarine forces (i.e., reside above state 1c on the spectrum displayed in Figure 1).

3. TFZ Identification and Analysis

We propose a simple, empirically based means to estimate the TFZ critical locations (λ_{fb}, λ_v, and λ_{st}, defined in section 2) as they evolve in response to tides and hydrology. Although the methods are designed for TFZs

Table 1
Varying Degrees of Tidal and Riverine Dominance Distinguish Four River Segments Separated by λ_{fb}, λ_v, and λ_{st}

Segment[a]	Water column chemistry	Discharge	Surface water stage	Dominant controls	TFZ critical point
a	Brackish or saline	Bidirectional	Tidal	Tide > > River	
					λ_{fb}
b	Fresh	Bidirectional	Tidal	Tide > River	
					λ_v
c	Fresh	Unidirectional	Tidal	Tide < River	
					λ_{st}
d	Fresh	Unidirectional	Riverine	Tide << River	

[a]a–d correspond to the labeled river segments in Figure 1b.

generally, they are explained within the context of an illustrative case study of the Aransas River (Texas, USA), monitored between July 2015 and July 2016 (section 4). Over this period, the Aransas River TFZ experienced large rainfall-runoff events, prolonged drought periods with minimal baseflow, and semidiurnal to semiannual tidal harmonics.

Data from the six monitoring stations (United States Geological Survey [USGS] and installed A1–A5) were linearly interpolated along the river to provide a spatial continuum of time series data for velocity, stage, and salinity (Figure 2). Using a 24-h moving window centered on each timestamp (i.e., on each field measurement, made every 15 min), we identified the locations of λ_{fb}, λ_v, and λ_{st} where interpolated conditions within the 24-h window matched the appropriate definition. In other words, for every timestamp of field measurements, we estimated the locations of λ_{fb}, λ_v, and λ_{st} based on the surrounding 24-h observations and their spatial interpolation. This resulted in a continuous time series of λ_{fb}, λ_v, and λ_{st} location estimates and, thus, a time series of TFZ location, estimated size, and dynamic behavior.

3.1. Identifying the Freshwater Limit: λ_{fb}

To locate the downstream limit of the TFZ by the farthest downstream extent of a freshwater column, λ_{fb} (synonymous with the farthest upstream extent of brackish waters), we identified where the system salinity was 2.0 practical salinity units (PSU), as a median over 24 h. (Another time period may be more appropriate given a different analysis and research question. See section 5.4 for a discussion of the consequences of selecting different tidal periods.) This threshold is similar to other studies measuring and/or modeling salinity intrusion (e.g., Monismith et al., 2002). When the most downstream sensor at A5 was <2.0 PSU, we spatially interpolated salinity between A5 and an endpoint representing the Gulf of Mexico with a constant salinity of 35.0 PSU located 60 km downstream. We used the distant Gulf as the interpolation end-member because the salinity of the intervening bays is often similar to the salinities of the rivers following rain events (Bruesewitz et al., 2013), so the bays are not useful end-members.

The freshwater threshold of 2.0 PSU was chosen to ensure that λ_{fb} estimated the limit of estuarine saline intrusion and not input from evaporation-concentrated terrestrial waters. Due to the region's semiarid subtropical climate, evaporation can produce elevated salinities in otherwise fresh inland waters (Evans et al., 2012; Mooney & McClelland, 2012). Maximum observed salinity in the nontidal Aransas River (upstream of A1) during the year-long study was 0.81 PSU. Thus, for this analysis, a smaller salinity threshold for λ_{fb}, such as 0.5 or 1.0 PSU, was deemed insufficient to reliably and definitively identify observed salt as estuary sourced. We acknowledge that 2.0 PSU is on the high end of freshwater salinities; however, other studies have discussed freshwaters at similar salinities (e.g., Jeppesen et al., 1994; Schallenberg et al., 2003; Swenson et al., 2006).

3.2. Identifying the Limit of Bidirectional Flow: λ_v

To identify the farthest upstream extent of tidal bidirectional velocities, λ_v (synonymous with the farthest downstream extent of unidirectional river velocity), we defined unidirectional flow as occurring at a location where fluxes were directed downstream during ≥90% (i.e., more than 21 h) of a 24-h window of time. Bidirectional tidal flow was therefore defined as occurring if flow was upstream >10% of the time within 24 h. To locate λ_v between monitoring points, we linearly interpolated the 10th percentile of observed velocity data and defined λ_v at the interpolated root (i.e., where the 10th percentile equaled 0.0 cm s^{-1}). To

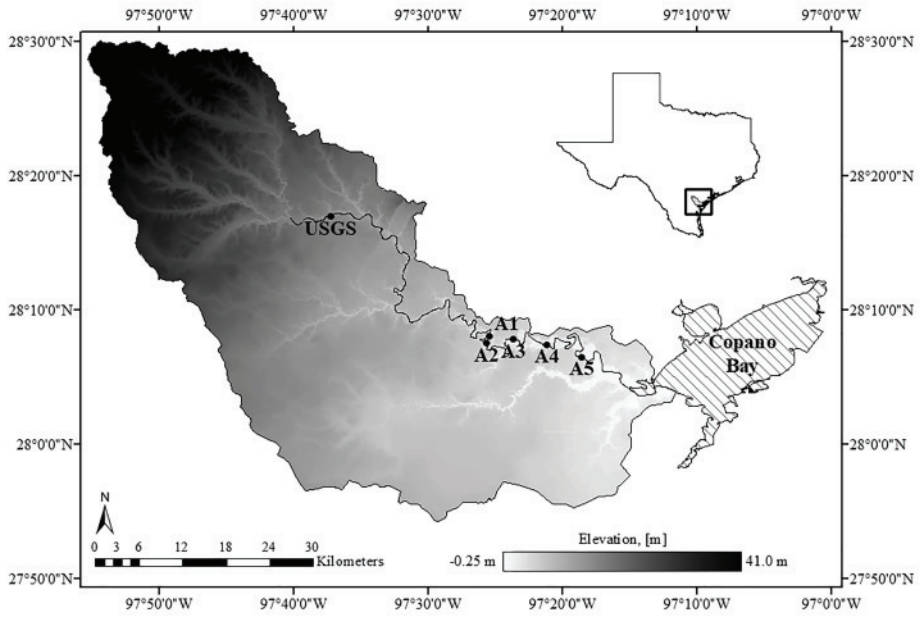

Figure 2. Map of monitoring sites A1–A5 installed along the Aransas River of southern Texas and the location of USGS gauge 08189700 (USGS, 2017). The along-river distances from the river mouth to each monitoring site are 94.6 km (USGS gauge), 45.5 km (A1), 43.1 km (A2), 34.6 km (A3), 28.1 km (A4), and 13.6 km (A5). Inset: Aransas watershed location within Texas, USA. Elevation data, watershed boundaries, and river lines were obtained from U.S. Geological Survey, National Geospatial Program (USGS, 2019).

approximate λ_v through extreme precipitation events (i.e., flash floods) where λ_v was pushed downstream of the river mouth, we linearly extrapolated the 10th percentile of velocity through sites A4 and A5 to 60 km downstream (the Gulf of Mexico endpoint). If the extrapolated values did not include 0.0 cm s^{-1}, then the location of λ_v was defined as the Gulf of Mexico endpoint.

3.3. Identifying the Limit of Tidal River Stage: λ_{st}

To identify the upstream limit of tidal water surface oscillations, λ_{st}, we divided the data into periods of baseflow and runoff-flooded river stage. Periods where river stage was elevated due to precipitation storm runoff events, rather than high tidal stage, are described as "storm" periods. Classifying the data into these two states (storm and baseflow) was necessary to avoid misinterpretation of stage changes, for example, the rising limb of a storm hydrograph versus a rising tide. A storm period was defined when the observed velocity exceeded the 90th percentile of tilt current meter (TCM) velocities measured at that site during the year-long study.

3.3.1. Storm Periods

To estimate the location of λ_{st} during storm periods, the timing of observed stage changes was compared against the timing of predicted tidal stage changes. If stage observations were approximately synchronized with predicted high and low tide (within ± ¼ tidal period), then a site was determined to be tidal and therefore downstream of λ_{st}. Sites whose observed stage was more asynchronous with tidal predictions were defined as nontidal and therefore upstream of λ_{st}.

Each monitoring site's tidal stage prediction was generated using a Real Fast Fourier Transform (RFFT) and frequency filter from the Python *numpy.fft* package. Filtering each site's recorded stage data isolated the site's five strongest stage-change harmonics. At each site along the Aransas River, the resulting harmonic frequencies (see supporting information A) matched those reported for neighboring Copano Bay (NOAA, 2017). An inverse RFFT recombined the five harmonics and their site-specific amplitudes to generate predictions of tidal stage for each riverine monitoring site, absent any storm effects.

Comparison of the timing of predicted and observed stage rate-of-change roots (i.e., $\frac{dS}{dt} = 0$ values) determined whether predictions and observations of high and low tide were synchronous. We derived $\frac{dS}{dt}$ time

series from predicted and observed stages using the field sampling interval of 15 min as dt between time$_n$ and time$_{n+1}$.

As the balance of riverine and tidal forces shifts throughout a precipitation event, the location of λ_{st} also changes. Thus, we analyzed each storm timestamp to determine the location of λ_{st} at that time relative to each monitoring site (i.e., site is upstream or downstream of λ_{st}). Within the 24 h surrounding each storm timestamp (i.e., timestamp ±12 h), we compared the timing of the predicted and observed $\frac{dS}{dt}$ roots. If ≥50% of observed roots were synchronous with the predicted roots (i.e., within ±3 h or ¼ of a semidiurnal tidal cycle), the site was classified as tidal and downstream of λ_{st} at that time; otherwise, the site was asynchronous, riverine, and upstream of λ_{st}.

Predicted and observed $\frac{dS}{dt}$ were linearly interpolated between the two monitoring locations immediately upstream and downstream of λ_{st}. The same synchrony analysis was then performed at regular intervals along that interpolated distance to determine a more precise location of λ_{st}. The location of λ_{st} for a given timestamp was recorded where the majority of interpolated $\frac{dS}{dt}$ roots transitioned from being tidally synchronous to asynchronous.

Although only a few roots exist in a given analysis window (e.g., 3 within a 24-h window), the roots convey more information than solely a pause (i.e., high or low tide) in tidal stage fluctuations. They also indicate transitions between periods of rising and falling stage, each of which indicate another aspect of a tide's signature. Thus, by comparing observed and predicted tidal roots, we in fact analyze both tidal motion and timing, which provides a simple, yet robust tidal characterization.

3.3.2. Baseflow Conditions

The above analysis was not necessary during baseflow conditions, because a simpler set of metrics could efficiently identify the location of notable stage oscillations, λ_{st}. During baseflow periods, λ_{st} was defined by the two-part requirement that sites downstream of λ_{st} should exhibit: (1) essentially zero average vertical velocity of the surface (i.e., rate of change of stage, $\frac{dS}{dt} \approx 0$) over 24 h, and (2) sufficiently large short-term changes in $\frac{dS}{dt}$ to indicate flood and ebb tides. Specifically, λ_{st} was estimated where the longitudinally interpolated 24-h median of $\frac{dS}{dt}$ was near zero and the 24-h $\frac{dS}{dt}$ interquartile range (IQR) exceeded a specified threshold related to a tidal range of ~5 cm. Since a practical, nonzero threshold of effective tidal stage extinction had to be selected, we selected <5 cm as a hydrologically and ecologically insignificant stage change for our purposes. In contrast, a sufficiently wide IQR describes significant periods of falling (negative $\frac{dS}{dt}$) and rising (positive $\frac{dS}{dt}$) stage, denoting substantial tidal influence with a range > 5 cm.

At each monitoring site, the dominant tidal period for the 24-h moving window in question was determined from a 24-h RFFT on the stage data. The harmonic with the stronger Fourier amplitude (12- or 24-h period) was isolated as the dominant tidal period. If diurnal, the site was denoted as downstream of λ_{st} if the $\frac{dS}{dt}$ IQR was >0.31 m d^{-1}; if semidiurnal, a $\frac{dS}{dt}$ IQR > 0.62 m d^{-1} classified a site as tidal and downstream of λ_{st}. These $\frac{dS}{dt}$ IQR thresholds reflect the tidal range threshold of 5 cm using the stage-rate-of-change calculations. We attempted to consolidate all thresholds into $\frac{dS}{dt}$ terms, so that only one variable space (i.e., $\frac{dS}{dt}$) would be necessary for the identification of λ_{st}. The method for determining the $\frac{dS}{dt}$ IQR thresholds for both semidiurnal and diurnal tides is presented in supporting information B; if the strongest contributing tidal harmonic at a site were of a different period, the analysis would be adjusted accordingly.

During baseflow conditions at our demonstration system's monitoring sites, the USGS gauge well upstream rarely exhibited a nonzero median $\frac{dS}{dt}$ (e.g., when minimal localized runoff was recorded by the gauge but did not overwhelm tidal influence). Under that circumstance, the interpolated longitudinal $\frac{dS}{dt}$ conditions inaccurately estimated the λ_{st} location as much farther downstream than it should have been. Under this rare condition, the nontidal gauge's nonzero median was either positive or negative, depending on conditions at the gauge. If positive, the 25th percentile of $\frac{dS}{dt}$ signified the return of tidal signal, whereas if the nonzero median were negative, the 75th percentile denoted significant tidal influence. In such rare cases, we estimated λ_{st} where the longitudinally interpolated 25th or 75th percentile crossed zero, representing the location where tidal conditions were present for at least one-quarter of the 24-h period around each analyzed time point. A more detailed guide to determining the location of λ_{st} can be found in supporting information A, including a workflow diagram for various conditions.

Table 2
Aransas River Tidal Freshwater Zone (TFZ) λ Locations (Kilometer Upstream From River Mouth) During Summer, Winter, and Over a Full Year

	λ_{fb}	λ_v	λ_{st}	TFZ length: (λ_{st}-λ_{fb})
Summer median	11.2	44.1	77.2	66.0
Summer mean	11.0	43.8	73.3	62.3
Summer standard deviation	0.6	0.3	11.3	-
Winter median	15.4	44.4	69.0	53.6
Winter mean	17.4	43.3	68.7	51.3
Winter standard deviation	5.2	0.4	10.6	-
Annual median	11.8	44.5	71.7	59.9
Annual mean	14.6	44.3	69.5	54.9
Annual standard deviation	5.4	0.8	11.6	-

3.4. Characterizing the TFZ

After determining the locations of each λ over time, we characterized the TFZ using a ratio of the bidirectionally flowing segment length to the entire TFZ length:

$$R = \frac{(\lambda_v - \lambda_{fb})}{(\lambda_{st} - \lambda_{fb})} \quad (1)$$

This ratio identifies whether a TFZ's discharge regime is primarily unidirectional ($R < 0.5$), bidirectional ($R > 0.5$), or balanced ($R \approx 0.5$) (Figure 4c).

These methods provide the locations of λ_{fb}, λ_v, and λ_{st} and analyze their spatial relationship to one another. They also ultimately describe the presence, reach location and length, and critical dynamic points of the TFZ. These methods were applied to the Aransas River, TX, USA to characterize and study the river's TFZ. The results of that demonstration case are presented and discussed in the following sections.

4. Demonstration Study Area and Results

4.1. Aransas River Field Area

The Aransas River is located in the southwestern portion of the Texas coastal plain, which is characterized by high summer temperatures (~ 34 °C) and mild winter temperatures (~ 9 °C). These high summer temperatures often result in annual evaporation (151.3 cm yr^{-1}) exceeding annual precipitation (88.6 cm $year^{-1}$) (Evans et al., 2012; Mooney & McClelland, 2012). Although drought conditions are common, warm summer waters of the Gulf of Mexico and El Niño Southern Oscillation (ENSO) events can lead to large, sporadic rains that promote regional flash flooding and coastal freshets (Mooney & McClelland, 2012; Ropelewski & Halpert, 1986; Wolter et al., 1999). As evidence of the region's hydrologic variability, from 1998 to 2008, the Aransas River discharge covered 6 orders of magnitude, from 6.5×10^{-3} to 829.7 $m^3\ s^{-1}$ (Evans et al., 2012). Tidal forcing, the Aransas River's shallow bed slope, and minimal baseflow were previously noted to produce a TFZ (Evans et al., 2012; Johnson, 2009; Jones et al., 2017; Mooney & McClelland, 2012).

4.1.1. Aransas River Field Monitoring

Five monitoring locations along the Aransas River (sites A1–A5, Figure 2) recorded thalweg velocity, stage, and electrical conductivity. At each site a SeaHorse TCM was anchored to the riverbed in the thalweg to record the magnitude and direction of flow. TCMs have been used to investigate bottom circulation and sediment dynamics in the Gulf of Maine (Aretxabaleta et al., 2014; Maio et al., 2016) and lagoonal current dynamics in the Mesquite, Aransas, and Copano Bays of the Mission-Aransas estuary (Tunnell et al., 2015). The TCM technology was considered appropriate here as it is (1) inexpensive and (2) robust in identifying changes in flow magnitude and tidal flow direction. Monitoring data were smoothed using a 6-h moving average to remove noise (e.g., wind) while preserving tidal and riverine signals.

4.1.2. Publicly Available Data

Nontidal river discharge and stage time series were obtained from the USGS National Water Information System for the Aransas River's farthest downstream freshwater gauging station (site number: 08189700) (USGS, 2017). From 1 July 2015 through 1 July 2016, the Aransas River experienced a relatively wet year including several large storms. The gauging station recorded a discharge minimum of 0.1 $m^3\ s^{-1}$, median of 0.2 $m^3\ s^{-1}$, mean of 0.4 $m^3\ s^{-1}$, and maximum of 36.0 $m^3\ s^{-1}$.

4.2. Seasonal TFZ Length Dynamics

The TFZ location and size in the Aransas River was identified over three periods: late summer (1 July to 1 September 2015), late winter (1 December 2015– to 1 March 2016), and a full year (1 July 2015 to 1 July 2016). The typical (median) length of the TFZ was calculated by obtaining the median λ locations over all time steps and then subtracting those overall medians ($\tilde{\lambda}_{st}$ - $\tilde{\lambda}_{fb}$) to determine the overall TFZ length (Table 2 and Figure 3). Alternatively, the median TFZ length could be determined from TFZ lengths of each timestamp. These two calculation methods showed negligible difference for our study.

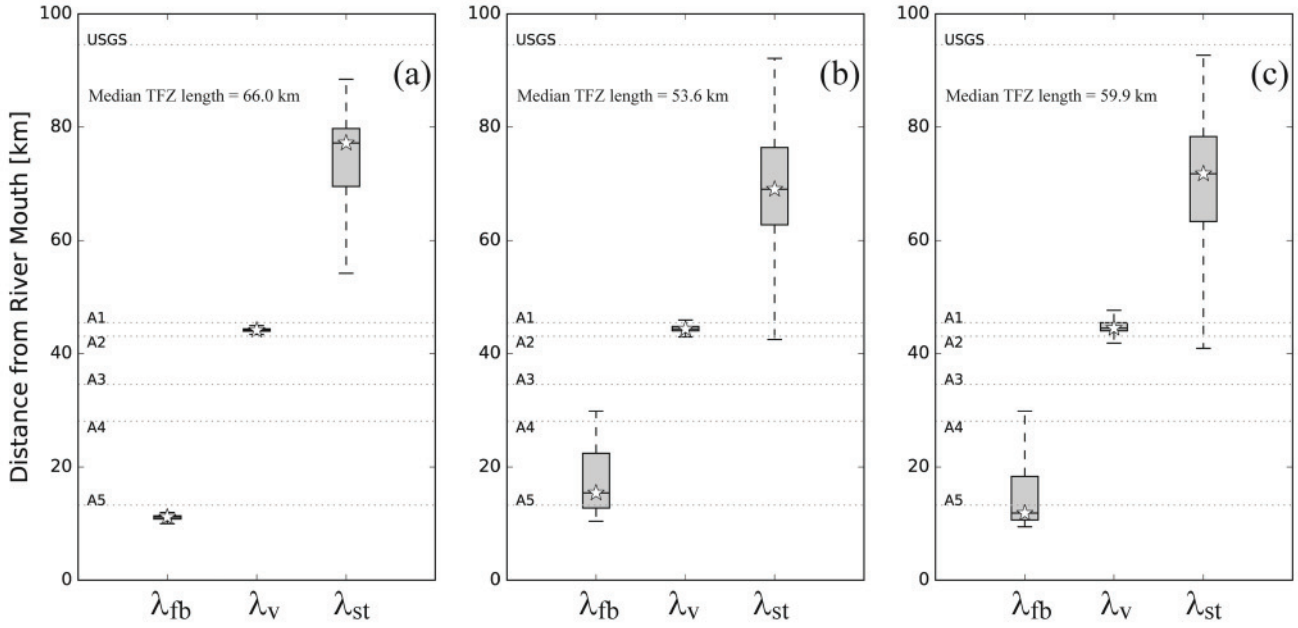

Figure 3. λ positions of the Aransas River TFZ, as median (star), interquartile range (box), and nonoutlier range whiskers for (a) late summer (1 July through 1 September 2015), (b) late winter (1 December 2015 through 1 March 2016), and (c) 1 year (1 July 2015 through 1 July 2016). The position of λ_{fb} steadily intrudes by salt transport upstream from summer to winter but varies with storm influence; λ_v remains fairly stationary; and λ_{st} varies widely due to spring-neap, annual tides, and storm influence.

In the late summer, the median TFZ length was 66.0 km. The late winter exhibited a shortened TFZ, with a median of 53.6 km. Over the full year, the median TFZ length was 59.9 km (Table 2 and Figure 3). The position of λ_{fb} moved upstream between the summer and winter time periods, from 11.2 to 15.4 km. The location of λ_{st} moved downstream between summer and winter, from 77.2 to 69.0 km. While the positions of λ_{fb} and λ_{st} shifted among the three time periods analyzed, the median position of λ_v changed a little (Table 2 and Figure 3).

4.3. Event-Driven Changes in TFZ Length

TFZ shortening and lengthening in response to storm and interstorm periods (Figure 4a) was observed in the TFZ length time series (Figure 4b). Five key runoff events during the year substantially lengthened the TFZ (marked by the dashed arrows between Figures 4a, 4b, and 4c). In the intervening time between each of these storms, the TFZ length decreased at a relatively consistent rate, associated with upstream translation of λ_{fb} via saline intrusion. The four interstorm time periods exhibited TFZ shortening rates of 0.2, 0.2, 0.4, and 0.3 km d^{-1} (Figures 4d–4g).

The Aransas River exhibited a median TFZ ratio, R, (equation 1) of 0.5 during the summer and winter months, but 0.6 over the monitored year, indicating that a slight majority of the TFZ consistently experienced bidirectional flow, while sporadic events promoted unidirectional regimes (Figure 4c).

5. Discussion

The goals of this study were fourfold: (1) gather and standardize a trans-disciplinary nomenclature for TFZs; (2) present a conceptual model and characterization of a TFZ's critical features; (3) develop methods for empirical identification of a TFZ and characterization of its overall temporal dynamics using simple and inexpensive field data; and (4) demonstrate the above, showing empirical temporal dynamics of a TFZ and its critical points λ_{fb}, λ_v, and λ_{st} as they respond to natural changes in precipitation, river discharge, and tide.

5.1. Controls on the Downstream Limit of the TFZ, λ_{fb}

Central to the TFZ definition, λ_{fb}, λ_v, and λ_{st} each delineate an important feature within the river-estuary continuum. The downstream boundary of the TFZ, λ_{fb} marks the extent of estuarine salt intrusion. Over

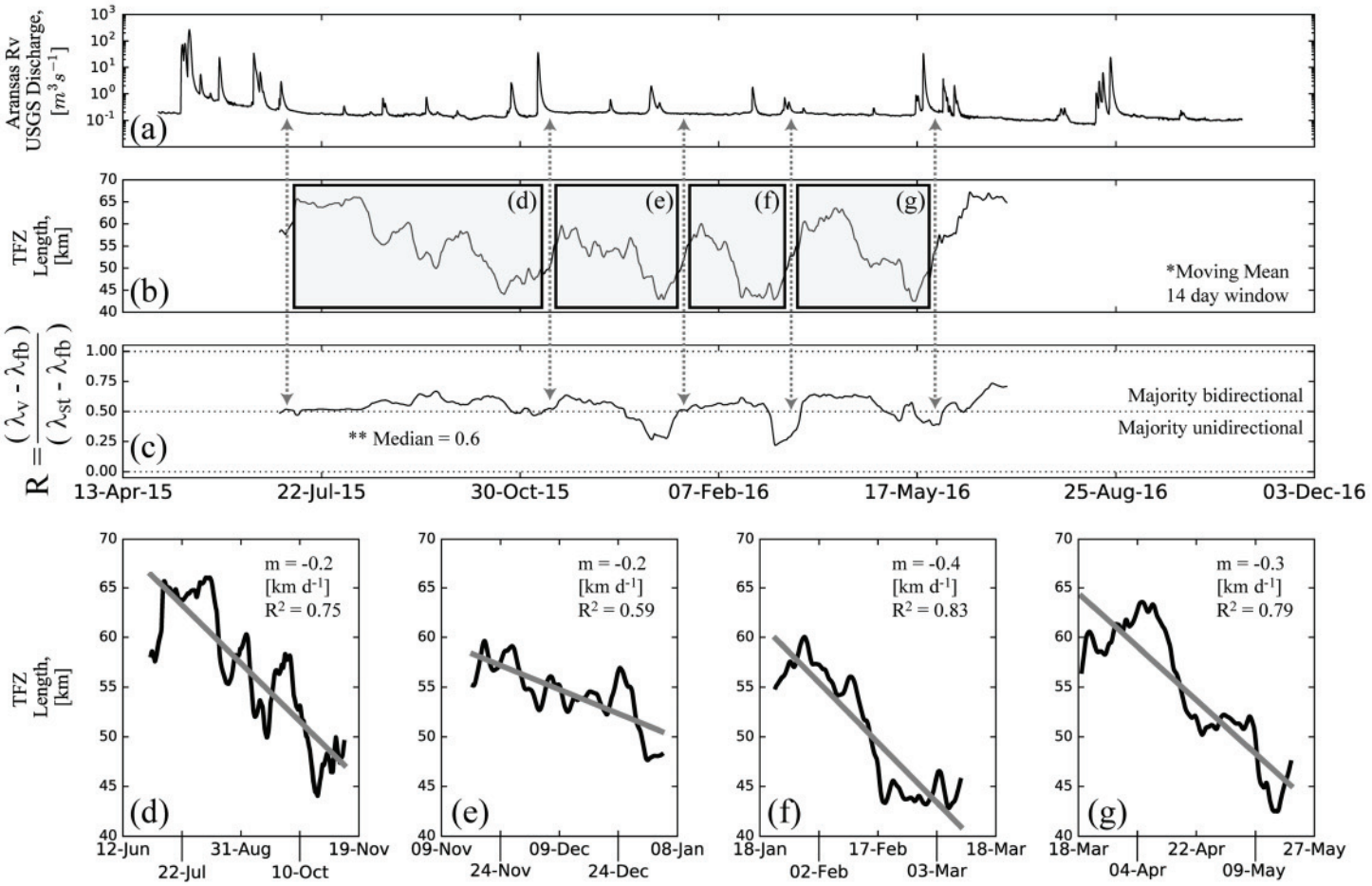

Figure 4. Time series of USGS gauge discharge (a) and the length of the Aransas River TFZ (b) from 1 July 2015 to 1 July 2016. The most influential storm events, marked by the dashed arrows between Figures 1a, 1b, and 1c, suddenly lengthened the TFZ. Some storms introduce large quantities of freshwater below the USGS gauge (e.g., third dashed arrow). Between those storms, the λs shifted relative to one another and so altered the proportion of the TFZ with bidirectional versus unidirectional flow (c). Between the storm-associated TFZ lengthening events, the overall TFZ shortened due to a fairly consistent upstream saline intrusion rate (d–g: 0.2, 0.2, 0.4, and 0.3 km d^{-1}).

extended periods of baseflow (months to years), the length of the TFZ is determined by the rate of upstream salinity intrusion, which shortens the TFZ over time. Salt transport upstream depends on the balance between river discharge, residual tidal currents from the upstream-oriented salinity gradient (gravitational circulation), and other dispersion forces (e.g., wind and shear) (Bowen, 2003; Fischer, 1976; Geyer & MacCready, 2014; Lerczak et al., 2006; MacCready & Geyer, 2010). The shortened Aransas River TFZ near the end of October 2015 (Figure 4b) was related to several months of minimal freshwater inflow that allowed relatively unimpeded saline intrusion. This saline encroachment shortened the TFZ segment that was fresh with tidal bidirectional velocity (i.e., segment **b** between λ_v and λ_{fb} in Figure 1b). Under opposite conditions, significant upstream freshwater input may elongate or even deconstruct the riverine TFZ by expelling λ_{fb} downstream beyond the river mouth, creating a freshwater plume (Figure 1a). Thus, a sufficiently wet season may cause a riverine TFZ to only exist during dry seasons, which may make the riverine TFZ a key seasonal, rather than continuous, occurrence.

Changes in the freshwater/brackish boundary (λ_{fb}) within the river-estuary continuum can cause substantial shifts in the ecology of affected reaches. For example, in Texas estuaries salinity is a main water-quality factor driving estuarine condition and, thereby, biological resource allocation (Palmer et al., 2011). In environments where salinity significantly correlates with live oyster abundance, extreme freshwater inputs such as flood discharges may reduce estuarine oyster population, spat settlement, and

filtration rates (Pollack et al., 2011). Thus, the location of λ_{fb} defines the divide between, and the extent of, habitats for species adapted to brackish or fresh waters.

5.2. Controls on the Unidirectional and Bidirectional Flow Transition, λ_v

The shift in discharge character along the TFZ length is denoted by λ_v, dividing the TFZ into a unidirectional discharge regime upstream (i.e., a tidally influenced river) and a bidirectional discharge regime downstream (i.e., a channelized freshwater estuary). Encapsulating the interaction between tidal, riverine, and geometric factors (e.g., channel roughness), λ_v marks where the freshwater and tidal momentums are functionally equivalent during the flood tide. The extent of the bidirectional discharge regime not only characterizes the maximum upstream extent of fine marine sediment deposition but also lengthens residence times in this lower portion of the TFZ (Burchard et al., 2018; Ensign, Doyle, et al., 2013; Ganju et al., 2004; Jones et al., 2017; Savenije, 2005).

In the water column, reaches downstream of λ_v experience small net transport over the tidal cycle due to relative flood/ebb tidal symmetry (Friedrichs, 2010; Friedrichs & Aubrey, 1988; Savenije, 2005), barring significant Stokes' drift (e.g., Cook et al., 2007; Dyke, 1980). For example, Ensign, Doyle, et al. (2013) analyzed three reaches of a TFZ in the Newport River (N. Carolina, USA), all downstream of λ_v, during a week in June 2008. From each site's average discharge, Ensign, Doyle, et al. (2013) calculated location-specific net transport rates during a tidal cycle of 0.03 m s^{-1} (downstream oriented) at the most upstream reach, 0.00 m s^{-1} at the middle reach, and − 0.03 m s^{-1} (upstream-oriented) at the most downstream reach. These reversed (upstream) velocity conditions downstream of λ_v suggest potentially long kinematic and solute residence times, which may alter local benthic biota and sediments (Ensign, Doyle, et al., 2013; Ganju et al., 2004; Ralston & Geyer, 2017; Savenije, 2005). In fact, net upstream sediment transport in reaches downstream of λ_v may be vital for maintaining the TFZ during periods of sea level transgression (Ensign et al., 2014).

The temporally variable TFZ length also provides insight into the range of residence times experienced within the TFZ. There is a natural relationship between residence time and system volume, assuming steady river flow conditions. Increases in system volume may relate to elongated residence times and vice versa (Jones et al., 2017). Thus, baseflow periods immediately following storm periods that lengthened the TFZ likely experience elongated residence times. Prior work in the Aransas River observed baseflow residence times of months to years for these tidal freshwater river reaches between intermittent storm periods (Johnson, 2009; Jones et al., 2017 ; Mooney & McClelland, 2012). Such residence times, dependent on both TFZ volume and river discharge, likely alter biogeochemical and sediment loads before being discharged to the estuary. Although dependent on both discharge and system volume, Aransas River residence times are likely primarily controlled by river discharge, since observed variability in river discharge (~3 orders of magnitude) was greater than the variability observed in TFZ length (<2 orders of magnitude) (Jones et al., 2017; Mooney & McClelland, 2012). However, conceptually, another system could exist where these conditions are reversed, where TFZ volume plays the dominant role controlling residence times.

The extent of tidal bidirectional discharge may alter biogeochemical processes as well, since bidirectional water transport may increase the amount of hyporheic exchange (Bianchin et al., 2010; Knights et al., 2017). The tidal pumping and hyporheic exchange experienced within the TFZ is important for mitigating new inputs of nitrogen (N) from groundwater sources. Modeled N loads to coastal environments may presently inaccurately estimate total N export (Knights et al., 2017). We hypothesize, for future study, that the longer the TFZ's bidirectional segment from λ_{fb} to λ_v (segment **b** in Figure 1b), and so the larger value of R (equation 1), the greater the opportunity for biogeochemical processes and loads to be altered before discharging into the downstream estuary. Negligible net discharge of TFZs may control the timing, magnitude, and composition of terrestrial nutrients discharging to coastal systems (Ensign et al., 2008; Knights et al., 2017; Mooney & McClelland, 2012). Future and ongoing work in TFZs will inform our understanding of the biogeochemical processes occurring downstream of λ_v. Also, future work might benefit from an analysis comparing λ locations to aquatic or neighboring riparian ecology.

For the Aransas River demonstration case, the location of λ_v remained mostly unchanged throughout 1 year (Figure 3). This may be unique to the Aransas River, since the location of λ_v coincided with two bridges crossing the river (rail line and highway US-77). The bridges' columns, backfill, and construction significantly alter and constrain the natural channel dynamics and may impede the upstream propagation of

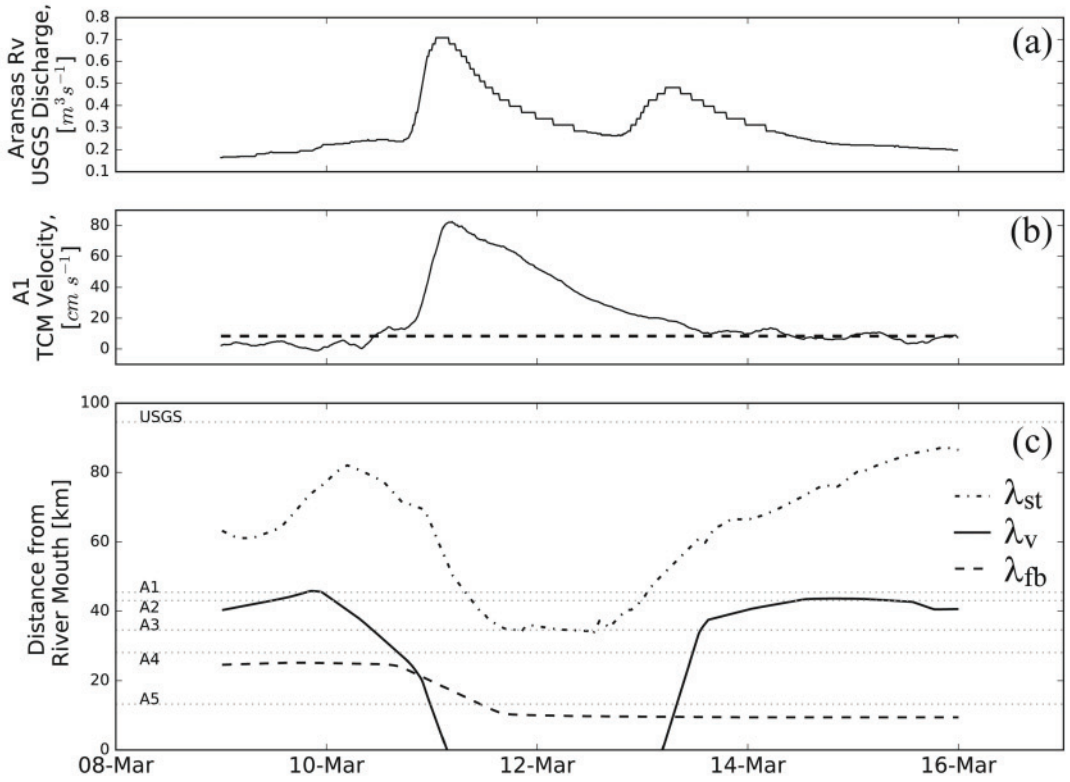

Figure 5. Storm flow inverted the positions of λ_v and λ_{fb} in the Aransas River in March 2016. Although the Aransas River USGS gauge did not record a dramatic peak in discharge on 11 March (a), a large amount of freshwater entered the system below the gauge and caused the TCM velocity at the most upstream installed site, A1 (b), to significantly exceed the annual 90th velocity percentile (dashed line in (b)), classifying the discharge as stormflow at A1 using this study's classification methodology. This large flow to the TFZ temporarily pushed λ_v downstream of λ_{fb} (c), as river flow overwhelmed tidal momentum (moving λ_v), yet estuarine salt was not fully extruded from the river (little movement in λ_{fb}).

tidal forces. However, the channel may have narrowed and impeded tidal forces at this location before construction. Torres (2017) observed several tidally influenced channels with decreased downstream cross-sectional area near the "current reversal limit" (their term, similar to λ_v) due to tidal backwater effects. Similarly, Ensign, Doyle, et al. (2013) investigated tidal freshwater channel morphology and observed that tidal hydrology greatly influenced bankfull channel cross-sectional area. Thus, channel geomorphology may provide insight into expected λ locations, since geomorphology will reflect the energy balance along the fluvial-tidal transition (Ensign, Doyle, et al., 2013; Torres, 2017; Yankovsky et al., 2012). Furthermore, channel geometry may also promote tidal reflections that augment the tidal influence from damping to zero (e.g., Friedrichs & Aubrey, 1994; Hoitink & Jay, 2016; Jay, 1991; Jay et al., 2016, 2015). Tidal reflections were not observed in the TFZ of the Aransas River and would be a useful area of future study.

Although in the Aransas River λ_v remained within the same reach through much of the study year, in general, the location of λ_v is transient. In some systems, λ_{st} and λ_v may overlap, creating a TFZ that has entirely bidirectional flow ($R = 1$, equation 1). Other systems may exhibit a substantial spatial separation between λ_{st} and λ_v, as in the Aransas River demonstration case, and may host a TFZ composed of two distinct discharge regimes ($0 < R < 1$). If R approaches zero, saline encroachment (λ_{fb}) has reached λ_v. These conditions may occur if large freshwater discharge translates λ_v downstream to reside near λ_{fb} (e.g., river-dominated end-member in Figure 1a) or if prolonged low-flow conditions allow estuarine saline waters to encroach upstream to λ_v. Large increases in riverine discharge can affect the momentum balance of the TFZ more quickly than the salt transport in the estuary and so may rarely push λ_v downstream to invert the positions of λ_{fb} and λ_v (Figure 5). Even small influxes may create an inversion of λ_{fb} and λ_v if persistent minimal

flow conditions allowed estuarine salt to intrude significantly upstream (i.e., move λ_{fb} upstream until $\lambda_{fb} \approx \lambda_v$, $R \approx 0$), but stormflow is insufficient to extrude λ_{fb}. Frequent λ_{fb}-λ_v inversions may occur in such special cases.

The latter portion of the inversion depicted in Figure 5 may be an artifact of our interpolation procedure. Without a monitoring station at the river mouth, the salinity gradient was quite steep between the interpolated endpoint of the Gulf of Mexico (35 PSU) and site A5. However, the portion of the inversion occurring before 12 March 2016 reflects the system dynamics and is not an artifact. This inversion occurred because λ_{fb} had steadily encroached upstream since January 2016, nearing λ_v, and increased discharge in March acted as a pressure pulse and forced λ_v downstream faster than salt was extruded (Figures 4f and 5). Thus, the water column observed in Figure 5 may have been strongly stratified with freshwater overlying saline waters (e.g., Savenije, 2005; Valle-Levinson, 2010).

If all three lambdas exist at the same location, then R is undefined and the system resembles the tide-dominated end-member in Figure 1c. A negative value of R indicates that λ_v is downstream of λ_{fb}, which may happen briefly during storm pulses. Mathematically, a negative ratio may also be obtained if λ_{st} were downstream of λ_{fb}; however, this situation may only apply in theory without extreme evaporation rates altering the river's salinity.

5.3. Controls on the Upstream Limit of the TFZ, λ_{st}

The upstream extent of tidal influence (λ_{st}) is controlled by river, tide, and channel geometry factors. The river state transition at λ_{st} may correspond to channel widening due to decreased energy dissipation and minimal sediment transport capacity, which promote channel bed aggradation (Ensign, Doyle, et al., 2013). The convergence rate of the channel's geometry strongly controls whether the tidal surface wave amplifies or dampens upstream (Friedrichs & Aubrey, 1994; Jay, 1991; Savenije, 2005). Tidal stage fluctuations will promote local tidal pumping, which will alter the volume of surface water-groundwater exchange compared to nontidal reaches upstream. Tidal pumping may be an important mechanism by which TFZ dynamics influence the freshwater channel bed's biogeochemistry (Chernetsky et al., 2010; Knights et al., 2017; Musial et al., 2016; Santos et al., 2009) and benthic ecology.

While channel geometry interacts with tidal propagation and groundwater exchange, frictional effects between the channel bed and tidal discharge interact with tidal amplitude to also influence λ_{st} (Godin, 1999, 1991; Kukulka & Jay, 2003). In the Aransas River, the semiannual low tide in the Gulf of Mexico (Ward, 1997) decreased the base level of the estuary during winter (December–February). The bed friction and slope then more effectively hindered the upstream movement of the tidal wave, which resulted in λ_{st} generally residing farther downstream in the winter than during the summer. The summer semiannual high tide may instead push λ_{st}, and potentially λ_{fb}, farther upstream due to the higher tidal base level, overcoming more of the river's energy gradient and channel's frictional effects.

At daily to fortnightly timescales the balance of river and tidal forces at λ_{st} controls TFZ length in the absence of stormflow. For the Aransas River, a Fourier transform on the λ_{st} location time series identified the strongest harmonic control on λ_{st} having a period of ~13.6 days, similar to fortnightly spring/neap tidal cycles (Figure 6).

On a similarly short timescale, λ_{st} also controls the reexpansion of the TFZ immediately after storm periods, for example, the transition from panel (f) to (g) in Figure 4b. The observed increase in TFZ length after stormflow is linked to the reestablishment of the typical balance of riverine and tidal forces during baseflow. As discharge returns to baseflow, λ_{st} is translated to its typical location upstream, which increases the TFZ length. However, the rate at which this poststorm expansion occurs is likely related to regional hydrology. For example, the semiarid Aransas River experiences brief, extreme runoff events and then quickly returns to low flow, that is, has a flashy discharge regime (Bruesewitz et al., 2013; Jones et al., 2017; Mooney & McClelland, 2012). Thus, the poststorm expansion observed between panels (f) and (g) of Figure 4b is relatively rapid (~10 days). TFZs in wetter climates will likely show more gradual poststorm lengthening if their storm hydrographs exhibit long-tailed recession.

Because they define the outer bounds of the TFZ, both λ_{st} and λ_{fb} impart control on the length of the TFZ. Through Figure 3, λ_{st} appears to impart a greater magnitude impact on the length of the TFZ. However, the smaller range of λ_{fb} locations may be limited by our ability to safely install a monitoring station at the

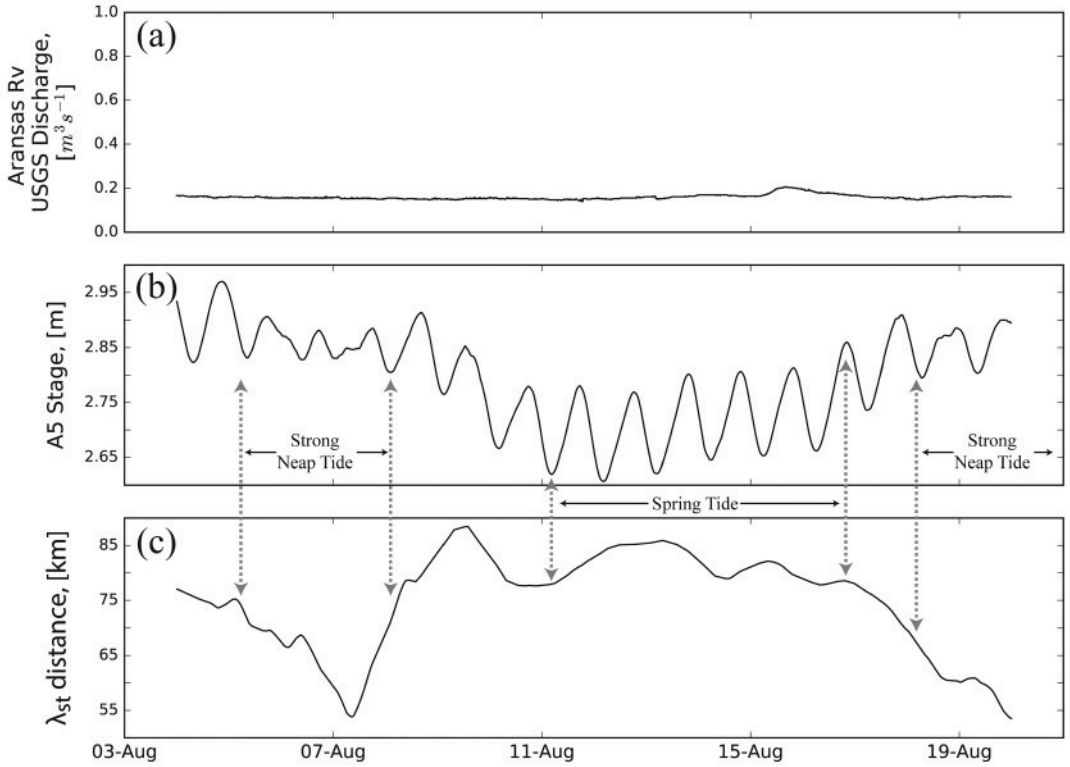

Figure 6. Temporal relations between spring and neap tides, and λ_{st}. During low baseflow at the USGS gauge (a), the most downstream monitoring site, A5, displayed strong tidal influence (b). Although located more than 50 km upstream of the river mouth, λ_{st} moved notably downstream during neap tide and upstream during spring tide (c).

Aransas River mouth and may relate to an artifact of our linear interpolation procedure to the Gulf of Mexico. Future iterations of this framework should work to refine our understanding of the relative magnitude of impacts of λ_{st} and λ_{fb}.

5.4. Empirical TFZ Identification Considerations and Caveats

The five inexpensive stage, salinity, and current monitoring sites installed along the Aransas River were sufficient to identify the local TFZ presence and position, associated TFZ critical points (λs), and the temporal nature of each, continuously throughout a year; however, some considerations are necessary. Alternative thresholds for λ identification could be used within the proposed framework to isolate more specific or unique dynamics of interest in other systems, while still respecting the conceptual definitions established here. For example, one could impose a more stringent analysis of λ_v position as occurring where 100% of flow is oriented downstream, rather than ≥90% as in our suggested framework (section 3.2), if the target of study is perhaps a benthic organism or freshwater intake orifice that cannot tolerate any changes in flow direction. The malleable functional definition and empirical analysis framework developed here can and should be adjusted depending on the research question and study system being interrogated.

Similarly, we defined λ_{st} as occurring where the surface water stage varied by not more than 5 cm during one tidal cycle, since a zero-change threshold is not a plausible empirical definition, but a different functional limit could be chosen. For example, Knights et al. (2017) examined tidal freshwater nitrification and denitrification rates down to a tidal range of 20 cm. Robins et al. (2015) modeled potential sites for converting tidal energy into electricity, with a model root-mean-square error of 15 and 5 cm for the amplitudes of the lunar (M2) and solar (S2) semidiurnal tidal constituents, respectively. Thus, our choice of a ≤ 5 cm amplitude threshold to define the position of λ_{st} was comparable to the amplitude uncertainty in a tidal water resource management model, but other studies may consider a different limit.

A key aspect of locating λ_{st} was distinguishing storm and baseflow periods. In systems lacking an annual hydrograph and where most hydrograph peaks correspond to major discharge events, such as with the Aransas River, a single velocity threshold for distinguishing storm and nonstorm flow may be sufficient (Bruesewitz et al., 2013; Mooney & McClelland, 2012). However, more complex methods for distinguishing λ_{st} during storm, nonstorm, and unique flow conditions may need to be developed when applying this TFZ conceptual model and lambda notation to additional locales. For example, continuous wavelet analysis (CWT) has been used to distinguish dominant tidal harmonics from dam hydropeaking (which produces a pseudotidal signal) and precipitation along the Columbia River (Hoitink & Jay, 2016; Jay et al., 2015). For systems with a cyclic annual hydrograph, an FFT might be used to predict annual discharge and isolate elevated nontidal stages. Future applications should be mindful of the hydrologic character of each system and end-users of the results and implement appropriate adjustments to our methods to identify λ_{fb}, λ_{v}, and λ_{st}, accordingly.

Another consideration for identifying λ_{st} is that some studies have observed fortnightly tidal fluctuations occurring upstream of daily tidal fluctuations (Hoitink & Jay, 2016; Jay & Flinchem, 1997; Nittrouer et al., 2012). Our λ_{st} time series for the Aransas River demonstration study included the effects of the fortnightly spring/neap variation but emphasized the extent and greater hydrological importance of daily tides as appropriate for this system and study. However, for larger rivers (e.g., Mississippi or Columbia, in the United States), these upstream fortnightly variations may have important influence. This could be addressed by including fortnightly (or other) tidal harmonics in the inverse RFFT used to predict tidal influence in this analytical framework (see section 3.3.1). Furthermore, when defining typical tidal conditions for determining λ locations, the analysis period should be carefully considered. While tides are described as "diurnal," which denotes a 24-h period (i.e., solar day), the period of the lunar tidal day is 24.8 h (NOAA, 2017). Thus, a 25-h period may be better suited for determining typical tidal conditions, or an alternative time period may be desired based on other study emphases (e.g., 12 h if studying the relation of day versus night ecological processes or a strongly semidiurnal system). Future iterations may also consider laterally expanding the conceptual model to incorporate neighboring ecosystems that adjoin the channel (e.g., wetlands), which may require different tidal harmonics and interpolation methods.

Another consideration is the choice in this study to linearly interpolate between monitoring sites to estimate λ locations for our demonstration of applying the TFZ framework. Interactions between channel geometry, tide, and river discharge may cause tidal forces to propagate upstream nonlinearly and may create other hydrogeomorphologic nonlinearities (Ensign, Doyle, et al., 2013; Friedrichs & Aubrey, 1994; Jay, 1991; Savenije, 2005). By linearizing the system within each reach (i.e., between each monitoring point), we essentially discretized longitudinal nonlinearities in the Aransas River into six linearized segments. Thus, this approach captures some longitudinal nonlinearity in the river segment of interest, but in a manner simple enough to apply for a wide range of potential users (e.g., ecologists, biogeochemists, water resource managers, watershed councils, and discharge permit analysts). Future iterations of the proposed framework could implement nonlinear interpolation methods (where appropriate) while remaining consistent with its definitions and logical approach. Furthermore, future iterations of this framework should carefully consider the spacing along the river reaches, and placement horizontally and vertically within a given river cross section, and choice of equipment installed to monitor the TFZ. For example, improper spacing of monitoring sites could result in interpolation procedures misrepresenting the physical system by simplifying, passing over, or not observing important hydrogeomorphologic variation.

6. Summary and Conclusion

This study defined a TFZ as a freshwater system characterized by freshwater chemistry and tidal physics. Empirical methods were developed to easily identify a reach containing a riverine TFZ and critical points within the TFZ using few and inexpensive field monitoring points. Aspects of hydrological and hydrodynamic theory that provide the basis for the TFZ and its critical points were discussed. This developed framework also suggests a lexical standardization around TFZs and aims to be easily applicable across diverse disciplines and a broad possible user base, to perhaps better facilitate accelerated, collaborative, interdisciplinary advancement of TFZ science and management.

In this standardized TFZ framework, the upstream limit of a TFZ, denoted λ_{st}, is defined where the daily interquartile range of surface water stage becomes less than a nominal threshold close to zero. The downstream limit of a TFZ, denoted λ_{fb}, is defined where river bed salinity transitions from fresh to brackish. An intermediate critical point in the TFZ, denoted λ_{v}, is defined where unidirectional river flow transitions to bidirectional tidal flow. These three TFZ critical points separate the discrete reaches that span the river-estuary transition (Table 1). The nondimensional parameter R, defined as the ratio of the length of the bidirectional TFZ segment to the total TFZ length, aids in the identification of the dominant flow character of a TFZ.

We demonstrated empirically locating the TFZ in the Aransas River of southern Texas and found that the location of λ_{st} was consistently controlled by local tidal harmonics, especially spring-neap and semiannual secular tides. Large storm events translated λ_{st} downstream until hydrograph recession enabled the return of λ_{st} upstream. The location of λ_{fb} in the Aransas River was controlled principally by gravitational circulation intruding saline estuarine waters upstream during baseflow periods at an average rate of 0.3 km d^{-1}. The location of λ_{v} in the Aransas River was relatively stationary over the study year. The Aransas River TFZ was closely balanced between unidirectional and bidirectional flow regimes, with R consistently near 0.5 despite the transient overall TFZ length. Over 1 year, the Aransas River TFZ had a mean length of 54.9 ± 13.2 km and a median length of 59.9 km.

The standardization of the defining characteristics of TFZs developed here may provide a unifying framework for drawing together observations of TFZ conditions in river systems around the world (e.g., Arndt et al., 2011, 2007; Cole et al., 1992; Findlay et al., 1991; Lovley & Phillips, 1986a, 1986b; Savenije, 2005). For example, more than 2,800 km of tidal freshwaters exist along the Middle Atlantic and Southeast Atlantic coastlines of the United States alone (Ensign & Noe, 2018) but have so far lacked a consistent set of descriptors to enable comparative study. The developed nomenclature and conceptual model may now enable examination of how prevalent TFZs are along global coastlines. The impacts of hurricanes on TFZs were not observed during this study but may be an area for future research (e.g., impacts of storm surge and increased precipitation on TFZ dynamics). There is also a need for further investigations into the residence time of TFZs (Jones et al., 2017) and its impacts on the timing, magnitude, and form of nutrients being transported to coastal environments (Knights et al., 2017; Mooney & McClelland, 2012). Such studies may inform policy decisions about environmental flows and total maximum daily loads reaching coastal environments, which are especially important as coastal populations and pollution threats grow (Destouni et al., 2008; Johnson, 2009; Knights et al., 2017; Neumann et al., 2015).

Acknowledgments
This work was supported by the U.S. National Science Foundation under grant EAR-1417433. Hodges was also partially supported by U.S. National Science Foundation grant 1331610. The data and parameters used in this study are listed in the manuscript, supporting information, or available from the cited public sources, and from the associated Consortium of Universities for the Advancement of Hydrologic Science, Inc. (CUAHSI) Hydroshare repository (Jones et al., 20192019). The supporting information provides additional details on identifying a TFZ and λ_{fb}, λ_{v}, and λ_{st}, including Python scripts used in the analysis. Substantial thanks to Craig Connelly, Xin Xu, Hengchen Wei, and Sarah Douglas of the University of Texas Marine Science Institute for their field assistance.

References

Aretxabaleta, A. L., Butman, B., Signell, R. P., Dalyander, P. S., Sherwood, C. R., Sheremet, V. A., & McGillicuddy, D. J. (2014). Near-bottom circulation and dispersion of sediment containing *Alexandrium fundyense* cysts in the Gulf of Maine during 2010–2011. *Deep Sea Research Part II: Topical Studies in Oceanography, Harmful Algae in the Gulf of Maine: Oceanography, Population Dynamics, and Toxin Transfer in the Food Web*, *103*, 96–111. https://doi.org/10.1016/j.dsr2.2013.11.003

Arndt, S., Lacroix, G., Gypens, N., Regnier, P., & Lancelot, C. (2011). Nutrient dynamics and phytoplankton development along an estuary-coastal zone continuum: A model study. *Journal of Marine Systems*, *84*, 49–66. https://doi.org/10.1016/j.jmarsys.2010.08.005

Arndt, S., Vanderborght, J.-P., & Regnier, P. (2007). Diatom growth response to physical forcing in a macrotidal estuary: Coupling hydrodynamics, sediment transport, and biogeochemistry. *Journal of Geophysical Research*, *112*, C05045. https://doi.org/10.1029/2006JC003581

Beardsley, R. C., Limeburner, R., Yu, H., & Cannon, G. A. (1985). Discharge of the Changjiang (Yangtze River) into the East China Sea. *Continental Shelf Research*, *4*, 57–76. https://doi.org/10.1016/0278-4343(85)90022-6

Bianchin, M., Smith, L., & Beckie, R. (2010). Quantifying hyporheic exchange in a tidal river using temperature time series. *Water Resources Research*, *46*, W07507. https://doi.org/10.1029/2009WR008365

Bowen, M. M. (2003). Salt transport and the time-dependent salt balance of a partially stratified estuary. *Journal of Geophysical Research*, *108*(C5), 3158. https://doi.org/10.1029/2001JC001231

Brock, D. A. (2001). Nitrogen budget for low and high freshwater inflows, Nueces estuary, Texas. *Estuaries*, *24*(4), 509–521. https://doi.org/10.2307/1353253

Bruesewitz, D. A., Gardner, W. S., Mooney, R. F., Pollard, L., & Buskey, E. J. (2013). Estuarine ecosystem function response to flood and drought in a shallow, semiarid estuary: Nitrogen cycling and ecosystem metabolism. *Limnology and Oceanography*, *58*, 2293–2309.

Burchard, H., Schuttelaars, H. M., & Ralston, D. K. (2018). Sediment trapping in estuaries. *Annual Review of Marine Science*, *10*, 371–395. https://doi.org/10.1146/annurev-marine-010816-060535

Chernetsky, A. S., Schuttelaars, H. M., & Talke, S. A. (2010). The effect of tidal asymmetry and temporal settling lag on sediment trapping in tidal estuaries. *Ocean Dynamics*, *60*, 1219–1241. https://doi.org/10.1007/s10236-010-0329-8

Cole, J. J., Caraco, N. F., & Peierls, B. L. (1992). Can phytoplankton maintain a positive carbon balance in a turbid, freshwater, tidal estuary? *Limnology and Oceanography*, *37*, 1608–1617. https://doi.org/10.2307/2838056

Cook, T. L., Sommerfield, C. K., Topher, K., & Wong, K.-C. (2007). Observations of tidal and springtime sediment transport in the upper Delaware estuary. *Estuarine, Coastal and Shelf Science*, *72*, 235–246. https://doi.org/10.1016/j.ecss.2006.10.014

Cowardin, L. M., Carter, V., Golet, F. C., & Laroe, E. T. (1979). Classification of wetlands and deepwater habitats of the United States (No. FWS/OBS-79/31). U.S. Department of the Interior, Fish and Wildlife Service, Office of Biological Services, Washington, DC. https://doi.org/10.1002/047147844X.sw2162

Destouni, G., Hannerz, F., Prieto, C., Jarsjö, J., & Shibuo, Y. (2008). Small unmonitored near-coastal catchment areas yielding large mass loading to the sea. *Global Biogeochemical Cycles*, *22*, GB4003. https://doi.org/10.1029/2008GB003287

Dyer, K. R. (1997). *Estuaries: A physical introduction* (2nd ed.). Chichester; New York: John Wiley.

Dyke, P. P. G. (1980). On the Stokes' drift induced by tidal motions in a wide estuary. *Estuarine and Coastal Marine Science*, *11*, 17–25.

Ensign, S. H., Doyle, M. W., & Piehler, M. F. (2013). The effect of tide on the hydrology and morphology of a freshwater river: Tidal river hydrology and morphology. *Earth Surface Processes and Landforms*, *38*, 655–660. https://doi.org/10.1002/esp.3392

Ensign, S. H., & Noe, G. B. (2018). Tidal extension and sea-level rise: Recommendations for a research agenda. *Frontiers in Ecology and the Environment*, *16*, 3743. https://doi.org/10.1002/fee.1745

Ensign, S. H., Noe, G. B., & Hupp, C. R. (2014). Linking channel hydrology with riparian wetland accretion in tidal rivers. *Journal of Geophysical Research: Earth Surface*, *119*, 28–44. https://doi.org/10.1002/2013JF002737

Ensign, S. H., Piehler, M. F., & Doyle, M. W. (2008). Riparian zone denitrification affects nitrogen flux through a tidal freshwater river. *Biogeochemistry*, *91*, 133–150. https://doi.org/10.1007/s10533-008-9265-9

Ensign, S. H., Siporin, K., Piehler, M., Doyle, M., & Leonard, L. (2013). Hydrologic versus biogeochemical controls of denitrification in tidal freshwater wetlands. *Estuaries and Coasts*, *36*(3), 519–532. https://doi.org/10.1007/s12237-012-9491-1

Evans, A., Madden, K., & Palmer, S. M. (Eds.) (2012). *The ecology and sociology of the Mission-Aransas estuary* (1st ed.). Port Aransas, Texas: Mission-Aransas National Estuarine Research Reserve.

Findlay, S., Pace, M., & Lints, D. (1991). Variability and transport of suspended sediment, particulate and dissolved organic carbon in the tidal freshwater Hudson River. *Biogeochemistry*, *12*(3), 149–169. https://doi.org/10.1007/BF00002605

Fischer, H. B. (1976). Mixing and dispersion in estuaries. *Annual Review of Fluid Mechanics*, *8*, 107–133.

Fong, D. A., & Geyer, W. R. (2002). The alongshore transport of freshwater in a surface-trapped river plume. *Journal of Physical Oceanography*, *32*, 957–972. https://doi.org/10.1175/1520-0485(2002)032<0957:TATOFI>2.0.CO;2

Friedrichs, C. T. (2010). Barotropic tides in channelized estuaries. In A. Valle-Levinson (Ed.), *Contemporary Issues in Estuarine Physics* (pp. 27–61). Cambridge: Cambridge University Press. https://doi.org/10.1017/CBO9780511676567.004

Friedrichs, C. T., & Aubrey, D. G. (1988). Non-linear tidal distortion in shallow well-mixed estuaries: A synthesis. *Estuarine, Coastal and Shelf Science*, *27*, 521–545. https://doi.org/10.1016/0272-7714(88)90082-0

Friedrichs, C. T., & Aubrey, D. G. (1994). Tidal propagation in strongly convergent channels. *Journal of Geophysical Research*, *99*, 3321. https://doi.org/10.1029/93JC03219

Ganju, N. K., Schoellhamer, D. H., Warner, J. C., Barad, M. F., & Schladow, S. G. (2004). Tidal oscillation of sediment between a river and a bay: A conceptual model. *Estuarine, Coastal and Shelf Science*, *60*, 81–90. https://doi.org/10.1016/j.ecss.2003.11.020

Geyer, W. R., & MacCready, P. (2014). The estuarine circulation. *Annual Review of Fluid Mechanics*, *46*, 175–197. https://doi.org/10.1146/annurev-fluid-010313-141302

Godin, G. (1991). Chapter 19—Frictional effects in river tides. In *Tidal hydrodynamics* (pp. 370–402). New York: J. Wiley.

Godin, G. (1999). The propagation of tides up rivers with special considerations on the upper Saint Lawrence River. *Estuarine, Coastal and Shelf Science*, *48*, 307–324. https://doi.org/10.1006/ecss.1998.0422

Hoitink, A. J. F., & Jay, D. A. (2016). Tidal river dynamics: Implications for deltas. *Reviews of Geophysics*, *54*, 240–272. https://doi.org/10.1002/2015RG000507

Jay, D. A. (1991). Green's law revisited: Tidal long-wave propagation in channels with strong topography. *Journal of Geophysical Research*, *96*, 20,585–20,598. https://doi.org/10.1029/91JC01633

Jay, D. A., Borde, A. B., & Diefenderfer, H. L. (2016). Tidal-fluvial and estuarine processes in the lower Columbia River: II. Water level models, floodplain wetland inundation, and system zones. *Estuaries and Coasts*, *39*(5), 1299–1324. https://doi.org/10.1007/s12237-016-0082-4

Jay, D. A., & Flinchem, E. P. (1997). Interaction of fluctuating river flow with a barotropic tide: A demonstration of wavelet tidal analysis methods. *Journal of Geophysical Research*, *102*, 5705–5720. https://doi.org/10.1029/96JC00496

Jay, D. A., Leffler, K., Diefenderfer, H. L., & Borde, A. B. (2015). Tidal-fluvial and estuarine processes in the lower Columbia River: I. Along-channel water level variations, Pacific Ocean to Bonneville dam. *Estuaries and Coasts*, *38*(2), 415–433. https://doi.org/10.1007/s12237-014-9819-0

Jeppesen, E., Søndergaard, M., Kanstrup, E., Petersen, B., Eriksen, R. B., Hammershøj, M., et al. (1994). Does the impact of nutrients on the biological structure and function of brackish and freshwater lakes differ? *Hydrobiologia*, *275*, 15–30. https://doi.org/10.1007/BF00026696

Johnson, S. L. (2009). *A general method for modeling coastal water pollutant loadings (Ph.D. dissertation)*. Austin, TX: The University of Texas at Austin.

Jones, A. E., Hodges, B. R., McClelland, J. W., Hardison, A. K., & Moffett, K. B. (2017). Residence-time-based classification of surface water systems. *Water Resources Research*, *53*, 5567–5584. https://doi.org/10.1002/2016WR019928

Jones, A., McClelland, J. W., Hardison, A. K., & Hodges, B. R. (2019). Monitoring a riverine Tidal Freshwater Zone (TFZ). HydroShare. http://www.hydroshare.org/resource/cb72a6f23d21459ab7fe9e72f55734b8

Knights, D., Sawyer, A. H., Barnes, R. T., Musial, C. T., & Bray, S. (2017). Tidal controls on riverbed denitrification along a tidal freshwater zone: Tides on riverbed denitrification. *Water Resources Research*, *53*, 799–816. https://doi.org/10.1002/2016WR019405

Kukulka, T., & Jay, D. A. (2003). Impacts of Columbia River discharge on salmonid habitat: 1. A nonstationary fluvial tide model. *Journal of Geophysical Research*, *108*(C9), 3293. https://doi.org/10.1029/2002JC001382

Lerczak, J. A., Geyer, W. R., & Chant, R. J. (2006). Mechanisms driving the time-dependent salt flux in a partially stratified estuary. *Journal of Physical Oceanography*, *36*, 2296–2311.

Lovley, D. R., & Phillips, E. J. P. (1986a). Organic matter mineralization with reduction of ferric Iron in anaerobic sediments. *Applied and Environmental Microbiology*, *51*(4), 683–689.

Lovley, D. R., & Phillips, E. J. P. (1986b). Availability of ferric iron for microbial reduction in bottom sediments of the freshwater tidal Potomac River. *Applied and Environmental Microbiology*, *52*(4), 751–757.

MacCready, P., & Geyer, W. R. (2010). Advances in estuarine physics. *Annual Review of Marine Science*, *2*, 35–58. https://doi.org/10.1146/annurev-marine-120308-081015

Maio, C. V., Donnelly, J. P., Sullivan, R., Madsen, S. M., Weidman, C. R., Gontz, A. M., & Sheremet, V. A. (2016). Sediment dynamics and hydrographic conditions during storm passage, Waquoit Bay, Massachusetts. *Marine Geology*, *381*, 67–86. https://doi.org/10.1016/j.margeo.2016.07.004

Monismith, S. G., Kimmerer, W., Burau, J. R., & Stacey, M. T. (2002). Structure and flow-induced variability of the subtidal salinity field in northern San Francisco Bay. *Journal of Physical Oceanography*, *32*, 3003–3019. https://doi.org/10.1175/1520-0485(2002)032<3003:SAFIVO>2.0.CO;2

Mooney, R. F., & McClelland, J. W. (2012). Watershed export events and ecosystem responses in the Mission–Aransas National Estuarine Research Reserve, South Texas. *Estuaries and Coasts*, *35*(6), 1468–1485. https://doi.org/10.1007/s12237-012-9537-4

Musial, C. T., Sawyer, A. H., Barnes, R. T., Bray, S., & Knights, D. (2016). Surface water-groundwater exchange dynamics in a tidal freshwater zone. *Hydrological Processes*, *30*, 739–750. https://doi.org/10.1002/hyp.10623

Neumann, B., Vafeidis, A. T., Zimmermann, J., & Nicholls, R. J. (2015). Future coastal population growth and exposure to sea-level rise and coastal flooding—A global assessment. *PLoS ONE*, *10*(3), e0118571. https://doi.org/10.1371/journal.pone.0118571

Nittrouer, J. A., Shaw, J., Lamb, M. P., & Mohrig, D. (2012). Spatial and temporal trends for water-flow velocity and bed-material sediment transport in the lower Mississippi River. *Geological Society of America Bulletin*, *124*, 400–414. https://doi.org/10.1130/B30497.1

NOAA (2017). Station selection—NOAA tides and currents [WWW Document]. NOAA Tides Curr. - Stn. Sel. URL https://tidesandcurrents.noaa.gov/stations.html?type=Water+Levels#Texas (accessed 6.1.17).

Odum, W. E. (1988). Comparative ecology of tidal freshwater and salt marshes. *Annual Review of Ecology and Systematics*, *19*, 147–176. https://doi.org/10.2307/2097151

Odum, W. E., Smith III, T. J., Hoover, J. K., & McIvor, C. C. (1984). The ecology of tidal freshwater marshes of the United States East Coast: A community profile (No. FWS/OBS-83/17), Community Profiles. U.S. Fish and Wildlife Service.

Palmer, T., Montagna, P., & Kalke, R. (2002). Downstream effects of restored freshwater inflow to Rincon bayou, Nueces Delta, Texas, USA. *Estuaries and Coasts*, *25*(6), 1448–1456. https://doi.org/10.1007/BF02692238

Palmer, T. A., Montagna, P. A., Pollack, J. B., Kalke, R. D., & DeYoe, H. R. (2011). The role of freshwater inflow in lagoons, rivers, and bays. *Hydrobiologia*, *667*, 49–67. https://doi.org/10.1007/s10750-011-0637-0

Pollack, J. B., Kim, H.-C., Morgan, E. K., & Montagna, P. A. (2011). Role of flood disturbance in natural oyster (*Crassostrea virginica*) population maintenance in an estuary in South Texas, USA. *Estuaries and Coasts*, *34*, 187–197. https://doi.org/10.1007/s12237-010-9338-6

Ralston, D. K., & Geyer, W. R. (2017). Sediment transport time scales and trapping efficiency in a Tidal River. *Journal of Geophysical Research: Earth Surface*, *122*, 2042–2063. https://doi.org/10.1002/2017JF004337

Robins, P. E., Neill, S. P., Lewis, M. J., & Ward, S. L. (2015). Characterising the spatial and temporal variability of the tidal-stream energy resource over the northwest European shelf seas. *Applied Energy*, *147*, 510–522. https://doi.org/10.1016/j.apenergy.2015.03.045

Ropelewski, C. F., & Halpert, M. S. (1986). North American precipitation and temperature patterns associated with the El Niño/Southern Oscillation (ENSO). *Monthly Weather Review*, *114*, 2352–2362. https://doi.org/10.1175/1520-0493(1986)114<2352:NAPATP>2.0.CO;2

Santos, I. R., Burnett, W. C., Dittmar, T., Suryaputra, I. G. N. A., & Chanton, J. (2009). Tidal pumping drives nutrient and dissolved organic matter dynamics in a Gulf of Mexico subterranean estuary. *Geochimica et Cosmochimica Acta*, *73*, 1325–1339. https://doi.org/10.1016/j.gca.2008.11.029

Savenije, H. H. G. (2005). *Salinity and tides in alluvial estuaries* (1st ed.). Amsterdam; Boston: Elsevier.

Schallenberg, M., Hall, C., & Burns, C. (2003). Consequences of climate-induced salinity increases on zooplankton abundance and diversity in coastal lakes. *Marine Ecology Progress Series*, *251*, 181–189. https://doi.org/10.3354/meps251181

Schuchardt, B., Haesloop, U., & Schirmer, M. (1993). The tidal freshwater reach of the Weser estuary: Riverine or estuarine? Netherland J. *Aquatic Ecology*, *27*(2-4), 215–226. https://doi.org/10.1007/BF02334785

Swenson, E. M., Cable, J. E., Fry, B., Justic, D., Das, A., Snedden, G., & Swarzenski, C. (2006). Estuarine flushing times influenced by freshwater diversions. *Journal of Coastal Conservation*, *33*, 403–412.

Torres, R. (2017). Channel geomorphology along the fluvial-tidal transition, Santee River, USA. *GSA Bulletin*, *129*, 1681–1691. https://doi.org/10.1130/B31649.1

Tunnell, J., Buskey, E. J., & Peterson, T. (2015). Freshwater inflows: Determining flow regimes in the face of land use change, climate change, and other unknowns (No. Final Report), National Estuarine Research Reserve System Science Collaborative. National Estuarine Research Reserve.

USGS (2017). USGS current conditions for Texas [WWW document]. Curr. Cond. USGS 08189500 Mission Rv Refug. TX. URL https://waterdata.usgs.gov/tx/nwis/uv/?site_no=08189500 (accessed 7.21.17).

USGS, 2019. The national map [WWW Document]. Natl. Map - Data Deliv. URL https://www.usgs.gov/core-science-systems/ngp/tnm--delivery (accessed 9.4.19).

Valle-Levinson, A. (2010). *Contemporary issues in estuarine physics*. Cambridge; New York: Cambridge University Press.

Von Korff, B. H., Piehler, M. F., & Ensign, S. H. (2014). Comparison of denitrification between river channels and their adjoining tidal freshwater wetlands. *Wetlands*, *34*, 1047–1060. https://doi.org/10.1007/s13157-014-0545-y

Ward, G. H. (1997). Process and trends of circulation within the Corpus Christi Bay National Estuary Program Study Area. Corpus Christi Bay Natl. Estuary Program CCBNEP-21.

Wolter, K., Dole, R. M., & Smith, C. A. (1999). Short-term climate extremes over the continental United States and ENSO. Part I: Seasonal temperatures. *Journal of Climate Boston*, *12*, 3255–3272.

Yankovsky, A. E., Torres, R., Torres-Garcia, L. M., & Jeon, K. (2012). Interaction of tidal and fluvial processes in the transition zone of the Santee River, SC, USA. *Estuaries and Coasts*, *35*(6), 1500–1509. https://doi.org/10.1007/s12237-012-9535-6